Icarus 215 (2011) 370–380

Contents lists available at ScienceDirect

Icarus

journal homepage: www.elsevier.com/locate/icarus

Radiolysis of sulfuric acid, sulfuric acid monohydrate, and sulfuric acid tetrahydrate and its relevance to Europa

M.J. Loeffler [a,*], R.L. Hudson [a], M.H. Moore [a], R.W. Carlson [b]

[a] Astrochemistry Laboratory, NASA Goddard Space Flight Center, Mail Code 691, Greenbelt, MD 20771, United States
[b] Jet Propulsion Laboratory, California Institute of Technology, Pasadena, CA 91109, United States

ARTICLE INFO

Article history:
Received 30 March 2011
Revised 7 June 2011
Accepted 8 June 2011
Available online 16 July 2011

Keywords:
Europa
Ices, IR spectroscopy
Jupiter, Satellites
Impact processes
Cosmic rays

ABSTRACT

We report laboratory studies on the 0.8 MeV proton irradiation of ices composed of sulfuric acid (H_2SO_4), sulfuric acid monohydrate ($H_2SO_4{\cdot}H_2O$), and sulfuric acid tetrahydrate ($H_2SO_4{\cdot}4H_2O$) between 10 and 180 K. Using infrared spectroscopy, we identify the main radiation products as H_2O, SO_2, $(S_2O_3)_x$, H_3O^+, HSO_4^-, and SO_4^{2-}. At high radiation doses, we find that H_2SO_4 molecules are destroyed completely and that $H_2SO_4{\cdot}H_2O$ is formed on subsequent warming. This hydrate is significantly more stable to radiolytic destruction than pure H_2SO_4, falling to an equilibrium relative abundance of 50% of its original value on prolonged irradiation. Unlike either pure H_2SO_4 or $H_2SO_4{\cdot}H_2O$, the loss of $H_2SO_4{\cdot}4H_2O$ exhibits a strong temperature dependence, as the tetrahydrate is essentially unchanged at the highest irradiation temperatures and completely destroyed at the lowest ones, which we speculate is due to a combination of radiolytic destruction and amorphization. Furthermore, at the lower temperatures it is clear that irradiation causes the tetrahydrate spectrum to transition to one that closely resembles the monohydrate spectrum. Extrapolating our results to Europa's surface, we speculate that the variations in SO_2 concentrations observed in the chaotic terrains are a result of radiation processing of lower hydration states of sulfuric acid and that the monohydrate will remain stable on the surface over geological times, while the tetrahydrate will remain stable in the warmer regions but be destroyed in the colder regions, unless it can be reformed by other processes, such as thermal reactions induced by diurnal cycling.

Published by Elsevier Inc.

1. Introduction

Remote sensing of Jupiter's icy satellites has revealed that even though their surfaces are composed mostly of water ice (Kuiper, 1957; Johnson and McCord, 1971), other molecules also are present, many of which are a consequence of the high radiation flux (Cooper et al., 2001) inducing surface chemistry. For instance, H_2O_2 on the surface of Europa (Carlson et al., 1999a), O_2 on the surface of Europa, Callisto and Ganymede (Spencer and Klesman, 2001; Spencer and Calvin, 2002) and O_3 on the surface of Ganymede (Noll et al., 1996) are all believed to be direct results of radiolysis of water–ice and its products. In addition, it has been suggested that detections of other species, such as SO_2 or CO_2, could also indicate radiolysis. SO_2 could have formed from implantation of Iogenic sulfur and subsequent reactions (Lane et al., 1981), while CO_2 may have formed via irradiation of water–ice on the surface of carbonaceous material (Hibbitts et al., 2000; Gomis and Strazzulla, 2005).

While radiolysis can produce many of the molecules on surfaces of the icy satellites, it is not the only way these molecules could have originated. For example, micrometeorite and cometary impacts could have brought exogenic material, such as CO_2, to the icy satellites (Hibbitts et al., 2000). In addition, the subsurface ocean proposed for not only Europa (Cassen et al., 1979) but also Ganymede (McCord et al., 2001a) and Callisto (Khurana et al., 1998) may be a source for some of the species detected. Material, possibly salty or acidic, could be transported to a surface by a variety of mechanisms as discussed by Kargel et al. (2000).

In light of these possible processes, the detection of distorted H_2O absorption features in the near-infrared spectra of Europa by the Galileo NIMS instrument has generated much interest. The distortion's cause is thought to be crystalline salt hydrates (McCord et al., 1999), hydrated sulfuric acid (Carlson et al., 1999b), or a combination of both (Orlando et al., 2005; Dalton, 2007). The presence of sulfuric acid (H_2SO_4) could be explained by radiation processes, while the salts could provide strong support for the putative ocean. Thus, determining whether salts, acid, or a combination of these species is present is very important for understanding surface and sub-surface geochemistry and is likely to influence the direction of future missions, modeling, and laboratory studies.

In the absence of sampling missions, the surest way to approach answering problems such as these are laboratory investigations. In fact, laboratory studies focusing on infrared (IR) spectra of ices and

* Corresponding author. Fax: +1 301 286 0440.
E-mail address: mark.loeffler@nasa.gov (M.J. Loeffler).

0019-1035/$ - see front matter Published by Elsevier Inc.
doi:10.1016/j.icarus.2011.06.008

molecules formed via radiation processes have been crucial in interpreting the remotely acquired spectra of satellite surfaces. For instance laboratory experiments have shown that ion irradiation of H_2O–ice (Teolis et al., 2006) and H_2O–O_2 ice mixtures (Baragiola et al., 1999) produces O_3 and H_2O_2 (Moore and Hudson, 2000; Gomis et al., 2004; Loeffler et al., 2006). Furthermore, it also has been shown that the spectrum of H_2O_2 on Europa's surface is matched by the laboratory spectrum of hydrogen peroxide dispersed in H_2O–ice (Loeffler and Baragiola, 2005).

While extensive IR spectral data are available for water ice in relevant astrophysical environments and over a range of wavelengths, much less has been published on salts and sulfurous materials in solid solutions. Mid-IR spectra of solids composed of pure H_2S and SO_2, as well as these same molecules mixed with H_2O, are in the literature (Salama et al., 1990; Schriver-Mazzuoli, 2003; Moore et al., 2007; Loeffler and Hudson, 2010). Mid-IR spectra of sulfuric acid and its hydrates (Middlebrook et al., 1993; Zhang et al., 1993; Moore et al., 2007) also have been published, while near-IR spectra are available for salt and sulfur hydrates (Carlson et al., 1999b; McCord et al., 2001b; Dalton, 2003, 2007; Dalton et al., 2005). Not surprisingly, there are fewer studies of radiation effects in salts and sulfurous materials under relevant astrophysical environments. UV photolysis and ion irradiation of SO_2 have shown that SO_3 is readily produced (Moore, 1984; Schriver-Mazzuoli et al., 2003; Garozzo et al., 2008). Electron irradiation of frozen S_8–H_2O mixtures produces SO_4^{2-} (Carlson et al., 2002). It has also been shown that ion irradiation and thermal annealing of H_2S–H_2O and SO_2–H_2O mixtures produces sulfuric acid and sulfuric acid hydrates (Moore et al., 2007), while other studies showed that S^+ ions implanted into water ice also produce hydrated sulfuric acid (Strazzulla et al., 2007) and possibly SO (Sack et al., 1992). Interestingly, little or no SO_2 was observed during the S^+ implantation into water ice (Strazzulla et al., 2007), which is the proposed mechanism for SO_2 formation on Europa (Lane et al., 1981). However, it is possible that SO_2 could form by the irradiation of salts or sulfuric acid, as SO_2 was observed in the gas phase during electron irradiation of $MgSO_4$ above 150 K, but was undetected at lower temperatures more typical of Europa (McCord et al., 2001b).

An interesting question that arises from these observations and experiments is whether salts and acids are thermally and radiolytically stable at the temperatures of the Galilean satellites. While there have been some studies on salts (Nash and Fanale, 1977; McCord et al., 2001b), there have been none on the radiation stability of solid sulfuric acid and its hydrates under Europa-like conditions. Therefore, in this paper we report investigations of the radiolytic stability of H_2SO_4, $H_2SO_4{\cdot}H_2O$, and $H_2SO_4{\cdot}4H_2O$, each of which has a distinct IR spectrum. Our experiments were conducted between 10 and 180 K with 0.8 MeV protons as the ionizing radiation. During irradiation we monitored the destruction of the starting material and the formation of products via IR spectroscopy. Finally, we have extrapolated our results to timescales relevant to the surface of Europa.

2. Experimental methods

2.1. Experimental setup and sample preparation

Experiments were performed in a stainless steel high-vacuum chamber with a thermal-radiation shielded cryostat ($T_{min} \sim 10$ K) and a base pressure under 1×10^{-7} Torr. Solid films of H_2SO_4, $H_2SO_4{\cdot}H_2O$, and $H_2SO_4{\cdot}4H_2O$ were made by two-step processes described below. Preparation of all samples began with the codeposition of H_2O and SO_2 onto a gold-coated aluminum mirror at 86 K using two separate pre-calibrated gas lines. The ice film's growth was monitored by recording interference fringes made by a diode laser (670 nm) at near-normal incidence (<5°). To prepare H_2SO_4 and $H_2SO_4{\cdot}H_2O$ samples, we started with 6:1 H_2O–SO_2 (3.6 ± 0.2 μm) ice mixtures, while to make $H_2SO_4{\cdot}4H_2O$ we began with 30:1 H_2O–SO_2 (2.9 ± 0.2 μm) ices. Thicknesses and number ratios were calculated assuming indices of refraction at 670 nm of 1.31 for H_2O (Warren and Brandt, 2008) and 1.36 for SO_2 (Musso et al., 2000), uniform mixing, and a density of 0.85 g cm^{-3} for H_2O and 1.46 g cm^{-3} for SO_2. Samples were grown at ~0.1 μm min^{-1}. We irradiated each ice sample with 0.8 MeV protons to a fluence of 1.6×10^{15} H^+ cm^{-2}. Fig. 1 shows representative IR spectra for a 6:1 H_2O–SO_2 ice mixture before and after irradiation, where it is clear that the SO_2 absorptions are almost completely lost as new features appear. The strongest bands have been assigned to H_3O^+ (1724 cm^{-1}) and SO_4^{2-} (1150, 983, and 620 cm^{-1}), while weaker ones have been attributed to HSO_4^- (1277 and 1052 cm^{-1}) and HSO_3^- (1225 and 1038 cm^{-1}) by Moore et al. (2007). Similar features were observed in the spectra of our irradiated 30:1 H_2O–SO_2 mixture (see Table 1 for initial peak positions of major absorption bands).

To prepare pure H_2SO_4, we warmed an irradiated 6:1 H_2O–SO_2 ice at 2 K min^{-1} to 235 K and held it there for 15 h to sublimate excess water, leaving amorphous H_2SO_4 behind. The resulting spectrum is labeled (a) in Fig. 2. Subsequent heating or cooling of the sample gave spectrum (b) of Fig. 2, where the sharpened lines indicate crystallization occurred, likely from the H_2SO_4 being a supercooled liquid near 235 K. However, since we were interested in measuring molecular destruction uncomplicated by structural changes such as amorphization, we preferred to begin with an amorphous sample. Therefore, after we obtained pure H_2SO_4 we warmed it to 290–295 K and then promptly cooled at the maximum rate of our system (6 K min^{-1}) to the desired irradiation temperature. Several factors caused the results to vary at this point. For instance, cooling more slowly or stopping the cooling above ~210 K caused the sample to crystallize. Also, the ice would only remain amorphous if a sulfur residue was present on the substrate, crystallizing during cooling if the substrate was clean. Thus, in our experiments with amorphous H_2SO_4 we had a residue beneath the acid, yet regardless of the residue's thickness our destruction data were reproducible to within ~5%. We note that thin sulfur films have negligible IR absorptions.

A modification of this post-irradiation warming procedure was used to prepare the two sulfuric acid hydrates. After irradiating the ice that originally had a 6:1 H_2O–SO_2 composition, we warmed the sample at 2 K min^{-1} to 195–200 K and held it there for about 15 h. During this time, excess H_2O sublimated while product molecules

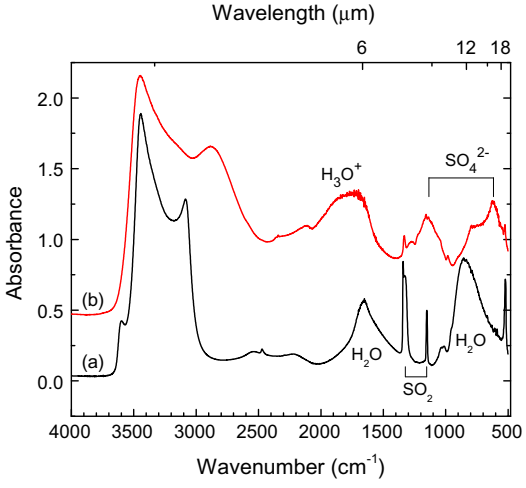

Fig. 1. Infrared spectra of a 6:1 H_2O–SO_2 mixture deposited at 86 K (a) before and (b) after irradiation with 1.6×10^{15} H^+ cm^{-2} at 86 K.

Table 1
Infrared positions (cm^{-1}) of ions and molecules identified in unirradiated ices at 86 K[a].

H_2SO_4	$H_2SO_4{\cdot}H_2O$	$H_2SO_4{\cdot}4\,H_2O$	Vibrational mode	Assignment
		3106	ν(O—H)	H_2O, $(H_5O_2^+)$, H_3O^+
	2940		$\nu_{as}S(O—H)_2$ $\nu(H_2O—H)$	HSO_4^-, H_3O^+
2809			$\nu_{as}S(O—H)_2$ $\nu_sS(O—H)_2$	H_2SO_4
2429			??	H_2SO_4
	2208		Overtone/combination	H_3O^+
	1730	1728	$\delta(H_3O^+)$	H_3O^+
	1645	1628	$\delta(H_2O)$	H_2O
1361		1222	$\nu_{as}(O=S=O)$	H_2SO_4
1142			$\nu_s(O=S=O)$	H_2SO_4
	1107		$\nu_{as}(SO_3)$	HSO_4^-
-		1064	$\nu_{as}(SO_4)$	SO_4^{2-}
	1008		$\nu_s(SO_3)$	HSO_4^-
955			$\nu_{as}(S—(OH)_2$	H_2SO_4
904			$\nu_s(S—(OH)_2$	H_2SO_4
		896	??	SO_4^{2-}
	893		$\nu(O_3S—OH)$	HSO_4^-
		590	$\delta(SO_4)$	SO_4^{2-}
	564		$\delta(SO_3)$	HSO_4^-
547			??	H_2SO_4

Also we note that δ = bending, ν = stretch, ν_{as} = asymmetric stretch, and ν_s = symmetric stretch.
[a] Assignments based on (Zhang et al., 1993; Horn and Sulley, 1999; Nash et al., 2001; Moore et al., 2007)

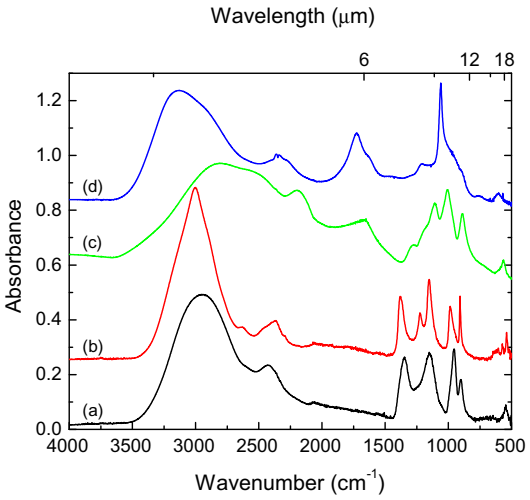

Fig. 2. Infrared spectra of sulfuric-acid ices formed by irradiation of a 6:1 H_2O–SO_2 mixture (30:1 H_2O–SO_2 mixture for tetrahydrate) and isothermal distillation: (a) amorphous H_2SO_4 at 240 K, (b) crystalline H_2SO_4 at 240 K, (c) crystalline $H_2SO_4{\cdot}H_2O$ at 200 K, and (d) crystalline $H_2SO_4{\cdot}4H_2O$ at 160 K. The spectra have been offset vertically for clarity.

and ions combined to form the monohydrate, which had the spectrum of (c) in Fig. 2. To prepare the sulfuric acid tetrahydrate, we warmed the more dilute (H_2O:SO_2 = 30:1) irradiated sample at 1 K min^{-1} to 160 K and left it there for 12–15 h. Under these conditions, the radiation products reacted and the majority of the excess water in the sample sublimated, yet the sample did not completely convert into $H_2SO_4{\cdot}4H_2O$. We next warmed this same sample at 3 K min^{-1} to 180 K, where it did convert into $H_2SO_4{\cdot}4H_2O$ in under 1 h; see (d) of Fig. 2 for the resulting spectrum. Our $H_2SO_4{\cdot}4H_2O$ samples were metastable under vacuum at 180 K, and had to be cooled to at least 160 K to prevent their conversion into $H_2SO_4{\cdot}H_2O$.

2.2. Initial sample composition

It is important to realize that while our two hydrates are written as simply $H_2SO_4{\cdot}H_2O$ and $H_2SO_4{\cdot}4H_2O$, crystallographic studies have shown that the monohydrate is actually $(H_3O^+)(HSO_4^-)$ (Taesler and Olovsson, 1968) and the tetrahydrate is $(H_5O_2^+)_2(SO_4^{2-})$ (Kjallman and Olovsson, 1972). In other words, the monohydrate ices we irradiated began with H_3O^+ and HSO_4^- present, while the tetrahydrate ices were composed of $H_5O_2^+$ and SO_4^{2-} ions. Unlike the two hydrates, our pure sulfuric acid samples show no evidence of autoprotolysis of the type

$$H_2SO_4 + H_2SO_4 \rightarrow H_3SO_4^+ + HSO_4^-$$

which may occur in liquid H_2SO_4 near room temperature. Thus, the amorphous H_2SO_4 ices we irradiated were molecular solids dominated by hydrogen-bonded H_2SO_4 molecules. Making these distinctions between the pure H_2SO_4 and hydrates is important for interpreting our results.

2.3. Irradiation techniques

We irradiated ice samples at normal incidence using a 1-MeV proton beam produced by a Van de Graaff accelerator. The ion beam was mass analyzed and sent through a nickel foil (thickness = 1 μm). This foil both spread out and randomized the beam and prevented the ice sample from cryopumping contaminants from the accelerator's vacuum system. We estimated that the proton beam lost about 0.2 MeV as it passed through the foil, giving 0.8 MeV for the energy of the ions at our samples. At this energy, the H^+ passed through our ices allowing us to measure their fluence (number of ions per cm^2) by integrating the current on the underlying metal substrate in real time and dividing by the area of the ion beam on the sample (3.75 cm^2). We note that our sample was biased at +48 V to minimize effects of secondary electron emission and that our beam current on the sample was 50 nA ($\sim 1 \times 10^{11}$ ions cm^{-2} s^{-1}).

Using SRIM2010 (Ziegler, 2010), we found that the energy deposited by 0.8 MeV protons was essentially constant across each ice sample's thickness. Specifically, the energy losses were 0.042 MeV μm^{-1} for H_2SO_4, 0.034 MeV μm^{-1} for $H_2SO_4{\cdot}H_2O$, and 0.027 MeV μm^{-1} for $H_2SO_4{\cdot}4H_2O$, assuming a pure sulfuric acid density of 1.86 g cm^{-3} and using a weighted average of densities. In addition, since our acid samples had different compositions, it was also useful to mass-normalize the radiation doses. One

method for doing this is to divide the energy absorbed in an ice by the number of molecules scaled to 16 amu, the mass of a typical small target molecule (e.g., CH_4), a convention first proposed by Strazzulla and Johnson (1991). For convenience, we refer to such radiation-dose units as simply "eV molecule^{-1}" in the present paper. Using this convention, along with our SRIM2010 results, we calculated that 1×10^{15} ions cm^{-2} deposit 6.07, 6.66, and 6.83 eV molecule^{-1} for H_2SO_4, $H_2SO_4{\cdot}H_2O$, and $H_2SO_4{\cdot}4H_2O$, respectively. We note that at the apex of Europa's trailing hemisphere a dose of 6 eV molecule^{-1} will be reached in ~3 years at a depth of 0.01 μm and about 20 years at 0.1 μm, considering only the proton flux at the surface (Paranicas et al., 2009).

2.4. Analytical technique and data analysis

The specular reflectance of the films on the gold-coated aluminum substrate was measured at an incident angle of 10°. The IR spectra were recorded with a Bruker Vector Fourier Transform infrared spectrometer at 2-cm^{-1} resolution over 8000–500 cm^{-1} as 100-scan accumulations. The spectra were divided by the reflectance of the gold mirror substrate taken before film deposition, and the resulting ratios, $R(\tilde{\nu})$, converted into absorbance, $-\log R(\tilde{\nu})$.

Absorption bands were integrated after subtraction of baselines that best matched the continuum on each side of an IR feature. While a linear baseline was reasonable at low radiation doses, where IR bands of reactants were strongest, it was unacceptable at higher ion fluencies as the reactant IR features were much smaller. In general, if the underlying continuum does not change shape (either curvature or slope) and an absorption band does not shift significantly during an experiment, then a non-linear continuum can be removed by subtracting each IR spectrum from the IR spectrum of the unirradiated sample. If this technique works, as it did for the $H_2SO_4{\cdot}4H_2O$ feature at 1065 cm^{-1}, then it will leave a baseline that can easily be removed with a straight line. This is particularly advantageous because it enables accurate quantification of band areas as IR features move below the continuum at high fluences. For pure H_2SO_4 (955 cm^{-1}) and $H_2SO_4{\cdot}H_2O$ (893 cm^{-1}) this technique did not work since the background continuum changed significantly during experiments. In these cases we simply fit each baseline with a non-linear background (dotted lines in Figs. 3 and 4). In addition for the pure H_2SO_4 experiments, we separated the overlapping features at 955 and 905 cm^{-1} (see Fig. 3) by fitting them with Gaussian functions. This was necessary since the band at 905 cm^{-1} overlapped with one of the bisulfate ion (HSO_4^-) features that formed during irradiation. Finally, in each experiment we normalized each band area by dividing it by the area of the relevant band in the initial spectrum of the unirradiated sample. This allowed us to compare experiments where the samples were a different thickness, which was a consequence of our sample preparation technique.

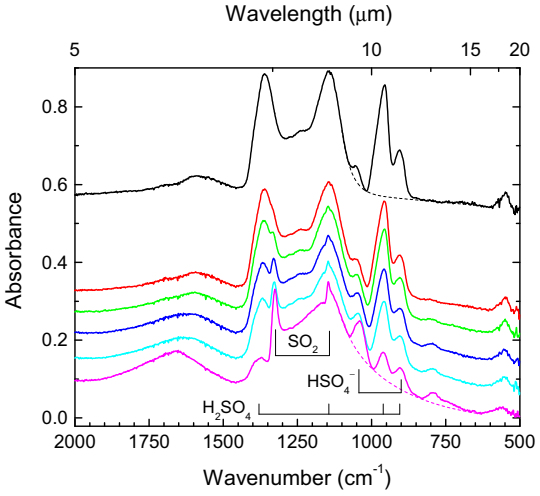

Fig. 3. Infrared spectra of amorphous H_2SO_4 during irradiation at 86 K with 0.8 MeV protons. Spectra from top to bottom are after 0, 0.14, 0.29, 0.54, 0.73, and 1.6×10^{15} H$^+$ cm^{-2}. Dashed lines in the top and bottom spectra show the backgrounds used to fit the absorption band at 955 cm^{-1}, which after deconvolving it from the overlapping 905 cm^{-1} band (see Section 2.4), was used to derive the relative abundance of sulfuric acid (see Fig. 7). The spectra have been displaced vertically for clarity.

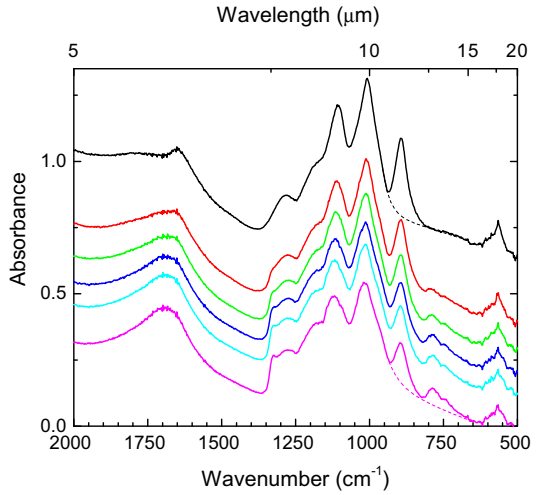

Fig. 4. Infrared spectra of crystalline $H_2SO_4{\cdot}H_2O$ during irradiation at 86 K with 0.8 MeV protons. Spectra from top to bottom are after 0, 0.14, 0.29, 0.54, 0.73, and 1.6×10^{15} H$^+$ cm^{-2}. Dashed lines in the top and bottom spectra show the backgrounds used to fit the absorption band at 893 cm^{-1}, which was used to derive the monohydrate's relative abundance (see Fig. 7). The spectra have been displaced vertically for clarity.

3. Results

3.1. Destruction of sulfuric acid and two sulfuric acid hydrates

We irradiated our H_2SO_4, $H_2SO_4{\cdot}H_2O$, and $H_2SO_4{\cdot}4H_2O$ samples with 0.8 MeV protons between 10 and 180 K. Figs. 3–5 show the evolution of the IR spectra of each sample irradiated at 86 K, Europa's minimum brightness temperature (Spencer et al., 1999), while Fig. 6 compares the infrared spectrum of each sample after irradiation at 10 K. For H_2SO_4, we observed the appearance of SO_2 through its ν_3 (1327 cm^{-1}) and ν_1 (1146 cm^{-1}) vibrations, the increase in the broad absorption at 1660 cm^{-1}, which is a combination of the bending mode of H_3O^+ and of water, as well as a band at 1020 cm^{-1}, likely the symmetric stretching mode of HSO_4^-. In addition, we also observe a broad band centered at 791 cm^{-1} that we identify as $(S_2O_3)_x$ (Hopkins et al., 1973).[1] The 1660 cm^{-1} and 1020 cm^{-1} bands show that the two ions of the monohydrate, namely H_3O^+ and HSO_4^-, were produced during irradiation of pure sulfuric acid.

Fig. 4 shows that proton irradiation of $H_2SO_4{\cdot}H_2O$ also produced SO_2 (1327 cm^{-1}), as well as an increase in intensity of the broad feature due to water and hydronium (1683 cm^{-1}), which is reasonably resolved at the beginning of the experiment but broadens with irradiation. In addition, an absorption at 785 cm^{-1} also

[1] We note that the possibility exists that this is $(S_2O_5)_x$ (see Reaction (15) in Section 4.1) but for simplicity we will refer to the identified species as $(S_2O_3)_x$ for the remainder of the text.

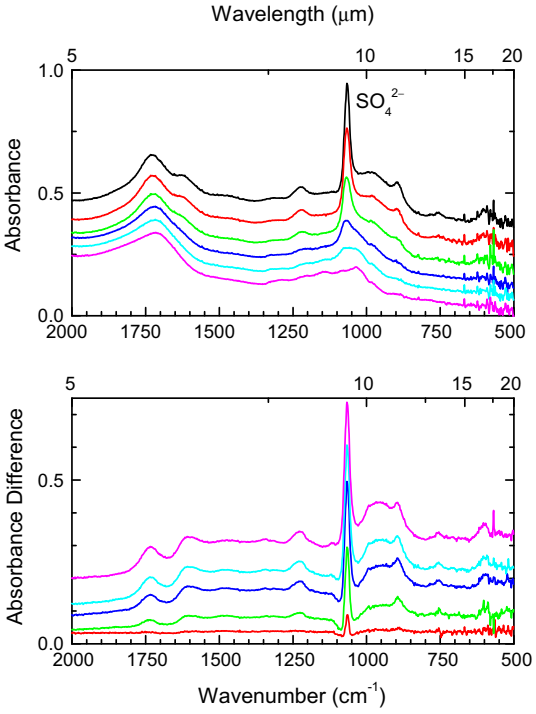

Fig. 5. IR spectra of crystalline $H_2SO_4{\cdot}4H_2O$ as a function of ion fluence at 86 K. In the upper panel the spectra are, from top to bottom, after 0, 0.038, 0.13, 0.28, 0.43, and 1.6×10^{15} H^+ cm^{-2}. The lower panel shows, bottom to top, the result of subtracting the zero fluence spectrum from each of the spectra in the upper panel. These traces in the lower panel were used to calculate the tetrahydrate's relative abundance (see Fig. 7), as this allowed us to more accurately choose the continuum at high doses. All spectra have been vertically displaced for clarity.

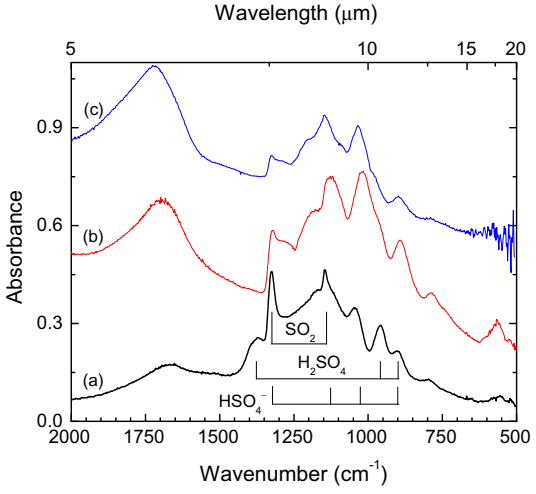

Fig. 6. Infrared spectra of: (a) H_2SO_4, (b) $H_2SO_4{\cdot}H_2O$, and (c) $H_2SO_4{\cdot}4H_2O$ after irradiation with 0.8 MeV protons at 10 K to a fluence of 1.6×10^{15} H^+ cm^{-2}. Identification of the main peaks in the S—O vibration region are given as vertical lines.

appeared, and likely is due to the same carrier as the band observed at 791 cm^{-1} in irradiated pure H_2SO_4 (Fig. 3).

For $H_2SO_4{\cdot}4H_2O$ ices, Fig. 5's upper panel shows (top to bottom) the spectra recorded after various radiation doses, while the lower panel shows (bottom to top) the spectra after the subtraction described in Section 2.4. In this sample, the amount of sulfate is expected to be significantly less, since we started with a H_2O–SO_2 mixture that was five times more dilute. This dilution likely contributes to the fact that we can barely detect the 1327 cm^{-1} SO_2

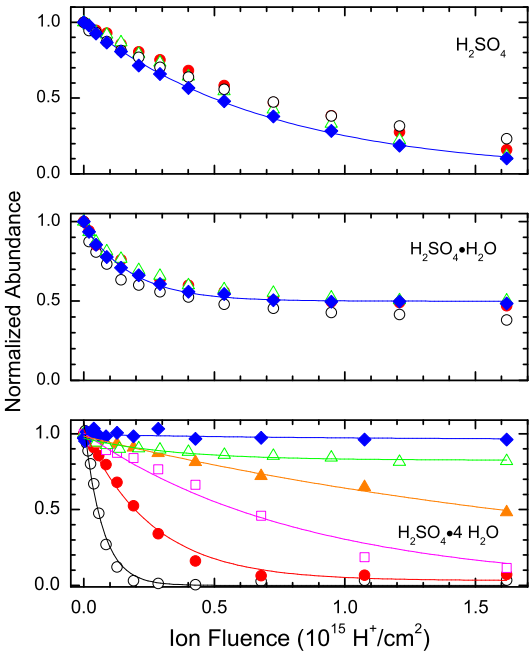

Fig. 7. Normalized abundances of H_2SO_4, $H_2SO_4{\cdot}H_2O$, and $H_2SO_4{\cdot}4\ H_2O$ as a function of ion fluence. The symbols are for experiments at 10 K (○), 86 K (●), 132 K (△), and 180 K (♦). In the bottom panel, the symbol (□) is for 110 K, (▲) is for 120 K and (♦) is for 145 K. Solid lines in the top and middle panels are fits for the 180 K data, while solid lines in the bottom panel show fits for each temperature. (For interpretation of the references to color in this figure legend, the reader is referred to the web version of this article.)

band and $(S_2O_3)_x$ band above the noise level. In fact, the spectral changes most easily observed were the broadening and attenuation of features assigned to the tetrahydrate, such as the SO_4^{2-} band near 1065 cm^{-1}. Finally, we note that in all experiments we also likely formed HSO_4^- or HSO_3^-, seen in H_2O–SO_2 mixtures; their IR bands were simply obscured by other features.

Fig. 7 shows the loss of the initial H_2SO_4, $H_2SO_4{\cdot}H_2O$, and $H_2SO_4{\cdot}4H_2O$ as a function of temperature and radiation dose. We irradiated the H_2SO_4 and $H_2SO_4{\cdot}H_2O$ ices at 10, 86, 132, and 180 K and found that the results were almost temperature independent. In contrast, we found that the destruction of the $H_2SO_4{\cdot}4H_2O$ depended strongly on temperature, as seen in the bottom panel of Fig. 7. We did not irradiate the tetrahydrate at 180 K, since it was unstable there (see Section 2.1). As seen in Fig. 7, the rate of change and overall shape of the destruction curves depended on each ice's original composition. For pure H_2SO_4, the decay did not reach an equilibrium at even our highest fluences, indicating that longer irradiations may completely destroy the H_2SO_4. For $H_2SO_4{\cdot}H_2O$, the decay was exponential and led to an equilibrium normalized abundance of ~0.5 for 86–180 K and a slightly lower value (~0.4) at 10 K. Finally, for $H_2SO_4{\cdot}4H_2O$ both the speed of the decay and the equilibrium abundance of the starting material depended on temperature, as below 110 K the band had dropped to less than 10% of its original value, while at our highest temperatures (145 K), the IR spectrum was almost unchanged. We will return to the temperature dependence of the tetrahydrate's decay in Section 4.3.

3.2. Formation of SO_2 and $(S_2O_3)_x$

Of the radiation products detected during our experiments, the two most-readily quantified are SO_2 and $(S_2O_3)_x$, which are clearly seen in both the pure H_2SO_4 and the monohydrate samples. Judging from the initial areas of absorption bands, the film thicknesses

of our pure H_2SO_4 ices were within 30% of each other, while the thicknesses of the monohydrate samples were even closer together (<10%). Thus, we can compare the total band area of the SO_2 and $(S_2O_3)_x$ formed as a function of temperature, which is shown for each sample in Figs. 8 and 9. For pure H_2SO_4, SO_2 formation does not depend on temperature, similar to the destruction results of Fig. 7, while more $(S_2O_3)_x$ is formed at higher temperatures. For $H_2SO_4{\cdot}H_2O$, more SO_2 is formed in the ice at lower temperatures,

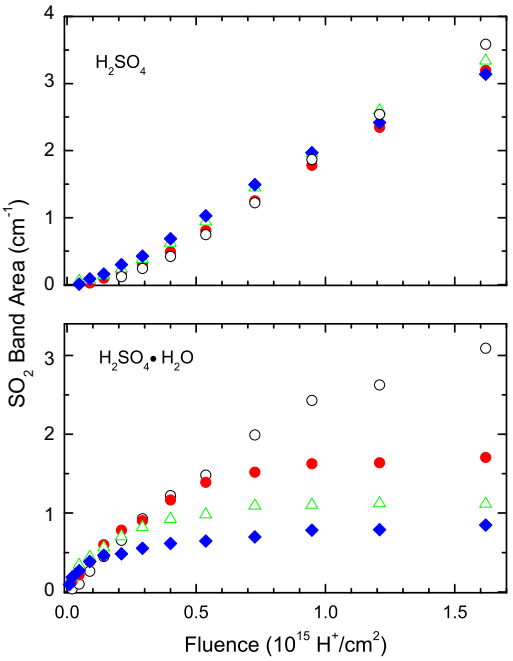

Fig. 8. Area of the 1327 cm^{-1} SO_2 band as a function of ion fluence for H_2SO_4 and $H_2SO_4{\cdot}H_2O$ with 0.8 MeV protons. Symbols denote data recorded at 10 K (○), 86 K (●), 132 K (△), and 180 K (◆). (For interpretation of the references to color in this figure legend, the reader is referred to the web version of this article.)

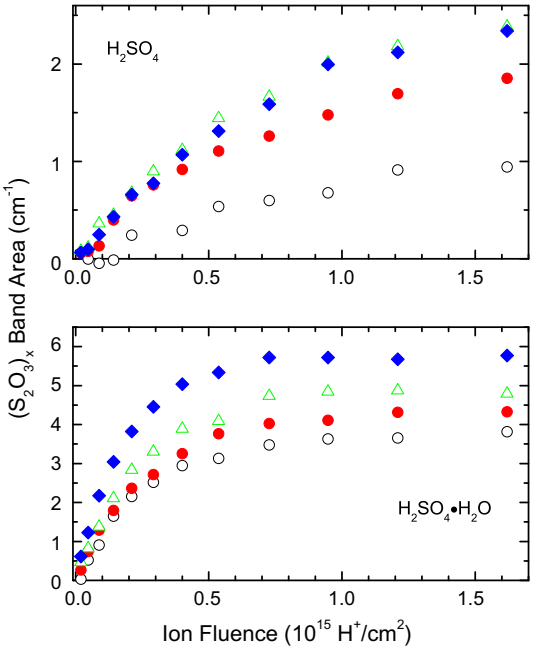

Fig. 9. Area of the 791 cm^{-1} $(S_2O_3)_x$ band as a function of ion fluence for H_2SO_4 and $H_2SO_4{\cdot}H_2O$ with 0.8 MeV protons. Symbols denote data recorded at 10 K (○), 86 K (●), 132 K (△), and 180 K (◆). (For interpretation of the references to color in this figure legend, the reader is referred to the web version of this article.)

while more $(S_2O_3)_x$ is formed at higher temperatures similar to the pure H_2SO_4 experiments. The SO_2 results are consistent with what was found in the tetrahydrate experiments, as the only temperature where we clearly observed SO_2 was 10 K (We found a smaller feature at 86 K and 110 K, barely above the noise level.). We note that it is unclear whether a similar trend is observed for $(S_2O_3)_x$ in the tetrahydrate sample, as although we did observe this feature at 10 K, we cannot detect it at higher temperatures due to the overlap of other absorptions that are not destroyed by irradiation. Finally, we note that we cannot quantitatively compare SO_2 and $(S_2O_3)_x$ formation in the three types of ices since their thicknesses differ. This thickness variation, and the accompanying optical interference effects, can change the effective band strength of absorption features (Teolis et al., 2007).

4. Discussion

4.1. Radiation pathways

Radiolysis of solids produces both neutral and ionic species capable of reacting by multiple pathways. Here we concentrate on those reactions that can explain the observed laboratory data, using standard treatments for condensed-phase radiation chemistry (Spinks and Woods, 1990) and earlier work on the radiolysis of aqueous H_2SO_4 solutions (Boyle, 1962). Beyond this, it is important to keep in mind that H_2SO_4 is a strong acid, reacting readily with H_2O molecules, even at cryogenic temperatures, as mentioned in Section 2.2.

Reactions in our ice samples were initiated by the incident protons and the secondary electrons they produced. For pure H_2SO_4, the expected reactions are as follows:

$$H_2SO_4 \rightarrow H_2SO_4^* \quad (1)$$

$$H_2SO_4 \rightarrow H_2SO_4^+ + e^- \quad (2)$$

The excited $H_2SO_4^*$ will relax to its ground state, but it can also dissociate into free radicals, and undergo molecular elimination:

$$H_2SO_4^* \rightarrow OH + HSO_3 \quad (3)$$

$$H_2SO_4^* \rightarrow H + HSO_4 \quad (4)$$

$$H_2SO_4^* \rightarrow H_2O + SO_3 \quad (5)$$

It also is possible that at 86 K the $H_2SO_4^*$ of reaction (3) will protonate a second H_2SO_4 to give $H_3SO_4^+$ and HSO_4^-, a reaction that corresponds to room-temperature autoprotolysis.

The radical cation of (2) also will play a role in the observed chemistry, undergoing an ion–molecule reaction with H_2SO_4 according to:

$$H_2SO_4^+ + H_2SO_4 \rightarrow H_3SO_4^+ + HSO_4 \quad (6)$$

to give the bisulfate radical (HSO_4) or it could recombine with an electron according to:

$$H_2SO_4^+ + e^- \rightarrow H_2O + SO_3 \quad (7)$$

Subsequent neutralization of the cation made in (6) will give both neutral and ionic products, as illustrated in the following reactions:

$$H_3SO_4^+ + e^- \rightarrow H_2O + HSO_3 \quad (8)$$

$$H_3SO_4^+ + e^- \rightarrow H_3O^+ + SO_3^- \quad (9)$$

$$H_3SO_4^+ + e^- \rightarrow H_2SO_4 + H \quad (10)$$

$$H_3SO_4^+ + e^- \rightarrow H_2O + SO_2 + OH \quad (11)$$

Of all the radicals and ions shown in these last reactions, it is the hydrogen atoms that will carry away the greatest kinetic energy, due to their low mass. Some of these atoms will combine with one another to make H_2, which in turn can escape from the ice sample. The hydrogen atoms also can undergo reactions with other radicals present. For example, reaction with HSO_4 simply regenerates the starting material, but reaction with bisulfite (HSO_3) according to:

$$H + HSO_3 \rightarrow H_2O + SO_2 \quad (12)$$

produces two observed products, and one, H_2O, is important for H_2SO_4 decomposition. Radical disproportionation involving HSO_3 can form SO_2:

$$HSO_3 + HSO_3 \rightarrow H_2SO_4 + SO_2 \quad (13)$$

The H_2SO_4 made either in reaction (10) or (13) will contribute to the spectrum of pure H_2SO_4, slowing the molecule's destruction, and also giving, by reaction with H_2O, the 1020 cm^{-1} absorption of HSO_4^- (bisulfate).

The molecular product $(S_2O_3)_x$ can be produced when SO, which forms from decomposition of SO_2 or any of the other sulfur oxyanions and radicals, reacts with various species such as in the following reactions:

$$SO + SO_2 \rightarrow S_2O_3 \quad (14)$$

$$SO + HSO_4 \rightarrow H + S_2O_5 \quad (15)$$

$$SO + HSO_3 \rightarrow S_2O_3 + OH \quad (16)$$

Reaction (14) has been used to explain an IR absorption feature formed from a discharge of gaseous SO_2 (Hopkins et al., 1973). Further irradiation is thought to polymerize S_2O_3, which would explain why more $(S_2O_3)_x$ is formed at higher temperatures. In addition, we note that Moore (1984) observed this absorption band and other higher wavenumber absorption features, also observed in other studies (Garozzo et al., 2008; Gomis and Strazzulla, 2008), and labeled it as poly(SO_3). However, we note that the extra sulfur atom (be it S_2O_3 or S_2O_5) is what causes the shift of this vibration from the 1000 cm^{-1} region, and the resulting SOS asymmetric stretch is found in essentially all molecules of the form X_nSOSX_n (Gillespie and Robinson, 1963).

Another ionic species that appears on irradiation of pure H_2SO_4 is hydronium (H_3O^+), which could be formed by reaction (9), but also by proton transfer from excited H_2SO_4 as shown below:

$$H_2SO_4^* + H_2O \rightarrow H_3O^+ + HSO_4^- \quad (17)$$

Any subsequent dissociation of the bisulfate (HSO_4^-) produced in reaction (17) will give additional hydronium along with sulfate (SO_4^{2-}):

$$HSO_4^- + H_2O \rightarrow H_3O^+ + SO_4^{2-} \quad (18)$$

Unlike many of the other reaction products already mentioned, H_3O^+ is stable at room temperature and is expected to remain in the ice on warming, as long excess water is present. The only reason we do not see it persist to ~298 K is that our warmings are done under vacuum, which results in removal of water to generate H_2SO_4 through the recombination of hydronium and bisulfate (see Section 2).

As a result of all of these reactions, an irradiated ice that is initially composed only of pure H_2SO_4 will contain a dose-dependent concentration of radicals (e.g., H, OH, HSO_3), stable molecules (e.g., H_2O, SO_2, $(S_2O_3)_x$, H_2), and stable ions (e.g., H_3O^+, SO_4^{2-}). It is all of these that give rise to the observed chemistry and spectral changes.

Turning to the two sulfuric-acid hydrates, as already mentioned they are commonly written as $H_2SO_4{\cdot}H_2O$ and $H_2SO_4{\cdot}4H_2O$, but actually are $(H_3O^+)(HSO_4^-)$ and $(H_5O_2^+)_2(SO_4^{2-})$, respectively. The literature shows that these hydrates can be prepared from, for example, cooling of solutions of the proper stoichiometry (Zhang et al., 1993) or exposure of H_2SO_4 to H_2O vapor (Horn and Sulley, 1999). In Section 2.1 we described our own procedure for warming an irradiated $H_2O + SO_2$ ice under vacuum to make $H_2SO_4{\cdot}H_2O$, but there is evidence that radiolysis of pure H_2SO_4 also produces the ions that form this same hydrate. Specifically, Fig. 3 shows the growth of the 1020 cm^{-1} feature of HSO_4^- and a broadening near 1700 cm^{-1} from H_3O^+, the two ions that constitute the monohydrate.

Figs. 6–9 compare the results of irradiating H_2SO_4 and $H_2SO_4{\cdot}H_2O$, and show that there are significant differences. First, radiolysis gives nearly-complete destruction of pure H_2SO_4 at high doses (Fig. 7), but under similar conditions the monohydrate's concentration reaches a non-zero equilibrium value. We suggest that the greater destruction of H_2SO_4 is from the multiple paths already outlined (i.e., radicals, acid–base, molecular elimination), whereas destruction reactions for the monohydrate (actually H_3O^+ HSO_4^-) are simply fewer in number and less efficient. For example, it might be possible for the H_3O^+ HSO_4^- pair to convert into $H_2SO_4 + H_2O$, but as H_2SO_4 is a strong acid the ion pair is expected to be much more stable than the two neutral molecules. Another possibility is the direct ionization of the original HSO_4^- of the hydrate. A likely sequence is the following:

$$HSO_4^- \rightarrow HSO_4 + e^- \quad (19)$$

$$HSO_4 + H_2O \rightarrow H_2SO_4 + OH \quad (20)$$

$$H_2SO_4 + H_2O \rightarrow H_3O^+ + HSO_4^- \quad (21)$$

Reaction (21) constitutes a back reaction that reforms the starting material, hindering its complete destruction. We note that the increased stability of H_2SO_4 in the monohydrate is also consistent with previous studies (Hochanadel et al., 1955) that show the production of SO_2 from H_2SO_4 aqueous solutions decreased as the concentration of water was increased.

Turning to $(S_2O_3)_x$ and SO_2, we see in Fig. 9 that $(S_2O_3)_x$ has similar temperature dependence in the monohydrate as compared to the pure H_2SO_4. In fact, at high fluences, the ratio between the band area of the samples at 180 K and 10 K compares well: 1.4 (H_2SO_4) vs. 1.5 ($H_2SO_4{\cdot}H_2O$), indicating that the addition of H_2O to the sample does not alter formation and destruction pathways of the S_2O_3 species significantly. SO_2, however, shows a much-stronger temperature dependence (Fig. 8) for the monohydrate compared to pure H_2SO_4. The source of this difference is difficult to determine, but it may be due to differences in abundance and mobility (Siegel et al., 1960; Plonka et al., 1984) of certain free radicals in each ice. Specifically, the yield of OH, from H_2O, radicals is expected to be greater for the monohydrate than for H_2SO_4, and such radicals could react by

$$OH + SO_2 \rightarrow HSO_3 \quad (22)$$

to efficiently destroy SO_2. As the irradiation temperature is increased above 10 K, increased OH radical mobility will mean that reaction (22) will decrease the observed SO_2 abundance, exactly as seen in the lower panel of Fig. 7. The relevance of a destruction mechanism such as reaction (22) and not a formation mechanism causing the temperature dependence observed for SO_2 is supported by the observation that the initial SO_2 production (where formation processes dominate) is temperature independent.

In addition to the molecules and ions already mentioned, other larger products such as H_2SO_5 or H_2SO_8 have been detected before in irradiated solutions (Boyle, 1962) and might form by similar reaction mechanisms in our own experiments through the following paths:

$$OH + HSO_4 \rightarrow H_2SO_5 \quad (23)$$

$$HSO_4 + HSO_4 \rightarrow H_2SO_8 \quad (24)$$

However, such products are difficult to detect with IR spectroscopy alone as their absorptions overlap with strong bands of other molecules and ions.

4.2. Destruction cross sections for H_2SO_4, $H_2SO_4{\cdot}H_2O$, and $H_2SO_4{\cdot}4H_2O$

We performed least-squares fits for the destruction data of Fig. 7 using an exponential decay of the form:

$$N = A\exp(-\sigma F) + N_\infty$$

where N is the normalized area of the IR feature selected, A is a pre-exponential factor, σ is a cross section (decay constant), F is the proton fluence in H^+ cm^{-2}, and N_∞ is the normalized area of the IR band of interest at infinite fluence. Table 2 summarizes the results of our calculations. We note that in a few cases, fitting produced $N_\infty < 0$, and so in those cases we fit our destruction curve using $N_\infty = 0$; these cases are marked (*) in Table 2. The destruction cross section (σ) for H_2SO_4 is on the order of 10^{-15} cm^2 with little temperature dependence. Furthermore, at high fluences N (normalized band area) tends to be below 0.1 and in some cases near zero. Destruction of the monohydrate was well fit by a single exponential decay in the experiments between 86 and 180 K, yielding a cross section near 5×10^{-15} cm^2 and $N_\infty \sim 0.5$. This same form for the decay equation did not fit the 10-K monohydrate data as well, although Fig. 7 shows that the decay rate resembles that at the other temperatures. Finally, trends for the tetrahydrate are more difficult to interpret if one looks only at the destruction cross section, because N_∞ also depends on temperature, specifically very little material is destroyed at 132 K ($N_\infty \sim 0.85$) and at 145 K ($N_\infty \sim 0.96$), while $N_\infty \sim 0$ for all experiments where $T < 132$ K. Thus in Table 3, we also show the irradiation dose (eV molecule^{-1}) needed to destroy half of each sample, where it is clear that the tetrahydrate is more stable at higher temperatures.

4.3. Interpretation of destruction cross sections

If the intensity of an IR feature falls during an experiment then one typically infers that the carrier's abundance has decreased and that the sample's overall composition has changed. These conclusions are reasonable for the irradiation of our pure amorphous H_2SO_4 ices, and thus the destruction cross sections reported in Table 2 can be interpreted as giving information directly on this molecule's destruction. However, this interpretation is potentially more complicated for the two hydrates studied, because these samples initially were crystalline. Thus, radiolysis not only produced the chemical changes already described, but may have also produced amorphization, altering the ice's spectrum without significant compositional changes (e.g., Hudson and Moore (1995)).

Table 3
Dose (eV molecule^{-1}) to reach $N = 0.5$ during irradiation of H_2SO_4 and two hydrates.

T (K)	H_2SO_4	$H_2SO_4{\cdot}H_2O$	$H_2SO_4{\cdot}4H_2O$
180	3	7.3	–
145	–	–	No[b]
132	3.6	6.0[†]	No[b]
120	–	–	10.9
110	–	–	4.1
86	4.3	7.3	1.4
10	4.3	3.1	0.3

[†] Here we show the dose needed to reach $N = 0.51$ rather than 0.50, since $N_\infty = 0.51$ (see Table 2).
[b] N has reached equilibrium well above 0.5 (see Fig. 7 and Table 2).

For the monohydrate, the IR bands did not change shape during irradiation, suggesting that either little amorphization took place at the temperatures chosen or that the spectra of the amorphous and crystalline materials were similar. Thus, the destruction cross sections and equilibrium values reported in Table 2 also give information directly on the monohydrate's destruction and stability.

For the tetrahydrate, the 1065 cm^{-1} feature did broaden significantly during irradiation (e.g., by the time half of the band area is lost at 86 K (Fig. 5), the band's FWHM has nearly doubled), suggesting that irradiation amorphizes the sample. Thus, the destruction cross sections and equilibrium values reported in Table 2 cannot be interpreted simply as the destruction of the sulfate ion, since amorphization likely contributes to the spectral changes observed during irradiation.

Determining the relative importance of amorphization and sulfate destruction for altering the infrared spectrum of the tetrahydrate is difficult. For instance, a similar temperature dependence – very little destruction at higher temperatures and more efficient destruction as the temperature was lowered – has been observed in the irradiation of other solids, such as water ice (Strazzulla et al., 1992; Hudson and Moore, 1995), suggesting that the spectral changes observed at lower temperatures could mainly be a structural effect. However, in contrast to previous amorphization experiments, at lower temperatures the band not only broadens but also disappears, indicating that the destruction of the sulfate ion is also important. The most likely pathway by which sulfate will be destroyed is as follows:

$$SO_4^{2-} \rightarrow SO_4^- + e^- \quad (25)$$

$$SO_4^- + H_2O \rightarrow HSO_4 + OH^- \quad (26)$$

$$HSO_4 + H_2O \rightarrow H_2SO_4 + OH \quad (27)$$

$$H_2SO_4 + H_2O \rightarrow H_3O^+ + HSO_4^- \quad (28)$$

An alternative to reaction (26) is the transfer of a hydrogen atom, as in the following:

$$SO_4^- + H_2O \rightarrow HSO_4^- + OH \quad (29)$$

Table 2
Equations for the radiolytic decay of H_2SO_4 and two hydrates.[a]

T (K)	H_2SO_4	$H_2SO_4{\cdot}H_2O$	$H_2SO_4{\cdot}4H_2O$
180	$0.98\exp(-1.4\times10^{-15}F)+0.01$	$0.48\exp(-5.5\times10^{-15}F)+0.50$	–
145	–	–	$0.04\exp(-1.1\times10^{-15}F)+0.96$
132	$1.01\exp(-1.19\times10^{-15}F)+0.00$[b]	$0.46\exp(-4.3\times10^{-15}F)+0.51$	$0.15\exp(-2.9\times10^{-15}F)+0.83$
120	–	–	$0.97\exp(-0.44\times10^{-15}F)+0.02$
110	–	–	$1.00\exp(-1.2\times10^{-15}F)+0.00$[b]
86	$1.0\exp(-1.04\times10^{-15}F)+0.00$[b]	$0.48\exp(-4.3\times10^{-15}F)+0.49$	$0.99\exp(-3.86\times10^{-15}F)+0.03$
10	$0.86\exp(-1.25\times10^{-15}F)+0.12$	$0.52\exp(-5.4\times10^{-15}F)+0.43$	$1.08\exp(-14.7\times10^{-15}F)+0.01$

[a] Each entry is for a least-squares fit of the data to an equation of the form $N = A\exp(-\sigma F) + N_\infty$ where N is the normalized area of the IR feature selected, A is a pre-exponential factor, σ is a cross section (decay constant), and F is the proton fluence (H^+ cm^{-2}). See the text for additional information.
[b] Indicates case where we forced $N_\infty = 0$ (see text for additional information).

If the decomposition products formed in (25) and (26) recombine more easily at higher temperatures, then sulfate decomposition could also explain the temperature dependence observed in our experiments.

Interestingly reactions (28) and (29) predict that the sulfate will decompose into bisulfate (HSO_4^-), which is the main sulfur anion in the monohydrate. There is spectral evidence supporting the formation of some bisulfate in Fig. 5 (top), as a weak feature at $\sim$1140 cm^{-1} appears in approximately the same position as one of the main HSO_4^- bands (the other two main features are obscured by the sulfate bands). Stronger spectral evidence for bisulfate production is shown in Fig. 6, which shows the IR spectrum recorded after irradiation at 10 K for all three samples studied. Clearly all three spectra are similar, as all show the three main absorptions indicative of HSO_4^- found in the monohydrate. The similarity among spectra is also expected at higher temperatures where the tetrahydrate signature is destroyed (T < 132 K) but only after higher irradiation doses than were studied here, since the decay of the sulfate feature is slower (Table 2).

5. Astrophysical implications

5.1. Enhanced SO_2 in Europa's chaotic terrains

Sulfur dioxide has been identified on trailing side of Europa and is thought to be part of radiolytic sulfur cycle involving sulfate, sulfur dioxide, and elemental sulfur (Carlson et al., 1999b). Europa's sulfur is due to implantation of sulfur ions from Iogenic plasma with possible contributions of sulfurous material from Europa's putative ocean. Our new results show that SO_2 as well as $(S_2O_3)_x$ are clearly produced by radiolysis of pure H_2SO_4 and the monohydrate ($H_2SO_4{\cdot}H_2O$) at temperatures relevant to Europa and that the SO_2 produced in the monohydrate depends on the irradiation temperature. We note that decomposition of $(S_2O_3)_x$ may also form SO_2, as molecules of the form $(S_2O_x)_y$ are unstable and have been shown to decompose both thermally and under irradiation to form polymeric sulfur, SO_2, SO_3, and O_2 in varying proportions that depend on the $(S_2O_x)_y$ formation conditions (Schenk and Steudel, 1965; Hapke and Graham, 1989; Steudel and Steudel, 2004; Baklouti et al., 2008; Gomis and Strazzulla, 2008).

In our tetrahydrate ($H_2SO_4{\cdot}4H_2O$) experiments, the SO_2 production decreased with increasing temperature as for the monohydrate and was not detected at temperatures characteristic of Europa, while the $(S_2O_3)_x$ feature is only barely detectable at 10 K. We cannot conclude from our experiments that the efficiency of production for either of these species is lower, since it could simply be a consequence of having less sulfur per unit volume. However, Hochanadel et al. (1955) showed that as the concentration of sulfuric acid was increased in liquid water solutions, the amount of SO_2 increased non-linearly, indicating that the SO_2/S abundance increased as the sulfuric acid became less hydrated. Similarly, Moore et al. (2007) found that the equilibrium SO_2/S ratio was generally higher in irradiated SO_2–H_2O mixtures that initially contained more SO_2 per unit volume.

Thus, our present laboratory studies combined with previous results show that the radiolytic production of SO_2 is temperature and composition dependent. In the following, we discuss recent measurements, which have found concentration variations of SO_2 over Europa's surface (Hendrix et al., 2011) in light of our results and propose that these variations may be indicative of recent thermal and geological activity.

Hendrix et al. (2011) have mapped the longitudinal profile of SO_2 in Europa's surface material, using numerous observations by the ultraviolet spectrometer (UVS) on Galileo. They find an overall pattern consistent with Iogenic sulfur implantation, but with regions of SO_2 enhancement that may correlate with regions of relatively recent geological activity. In particular, they found a concentration enhancement, of up to a factor of 5 over the average, near the center of the trailing side, a region of Europa's trailing hemisphere that includes the dark chaotic region Conemara Chaos along with dark bands Asterius Linae and Agave Linea (Schenk, 2010). Specifically, the enhanced SO_2 region was found during the 14ENICERAF01 ("Ice Raft") observation and covered the west longitude region 265–285° and the longitude range −2.5° to 12.5°. Hendrix et al. also found that the SO_2-rich area was very dark in the ultraviolet. The near-infrared mapping spectrometer (NIMS) on Galileo (Carlson et al., 1992) also obtained measurements during this sequence, particularly of Conerama and adjacent areas, which are discussed below.

Chaos terrains, for which Conerama Chaos is a striking example, generally are regions where an icy crust has been broken into numerous polygonal blocks, which have been further eroded, reoriented, and displaced (Collins and Nimmo, 2009). These once mobile blocks lie within an irregular, lumpy matrix and suggest that the matrix was once liquid or consisted of soft ductile ice. Various models of chaos formation have been proposed, including localized melt-through of a subsurface ocean, sub-surface cryomagmatic heating, or an impact event, but the common feature is heating of large areas of the crust and its sulfate-rich, tens-of-cm depth regolith (Carlson et al., 2009). As has been seen in our experiments and in our previous reports (Moore et al., 2007) heating the sulfuric acid hydrates even to moderate temperatures (160–250 K) will cause the H_2O to sublimate, hence increasing the sulfate concentration and decrease the average hydration state. Heating such as this can lead to a regolith that is rich in H_2SO_4, $H_2SO_4{\cdot}H_2O$, and elemental sulfur. Sulfur absorbs strongly in the ultraviolet, so this material will appear dark in the UVS spectral range. Radiolysis of this material will produce SO_2 in much greater quantities than highly hydrated surfaces. A simple heating process such as this, followed by radiolysis, would explain why the SO_2 concentration is enhanced in these chaotic regions, and it would also suggest that the average hydration state in this region would be lower than the overall average.

However, during the above-mentioned sequence (reexamined here) and on previous orbits, the Galileo NIMS 14ENICERAF01 spectra showed that the hydration state of the sulfuric acid inferred from infrared reflectance was no different than what was typically observed on the trailing side of Europa: 6–8 H_2O molecules bound to each sulfate ion (Carlson et al., 2005, 2009). This apparent discrepancy can be understood by considering that after the chaotic region forms, the surface will cool, during which time condensation from Europa's tenuous H_2O atmosphere will rehydrate the optical layer. For the observations described above, the surface temperature is too low for significant sublimation, so the main source of H_2O in the atmosphere will be from sputtering. Thus, equating the condensation rate with the sputtering rate, $\sim 10^9$ cm^{-2} s^{-1} or somewhat higher (Johnson et al., 2009), and assuming 100 μm for the optical depth, we find an optical surface rehydration time of $\sim 10^4$ years. If sublimation of water ice from the surface contributes to the atmospheric water, such as at the subsolar point (Johnson et al., 2009), then this time for rehydration would be reduced. As long as the SO_2 enhancement remains within the observed optical depth during this time, we can have a scenario that can be consistent with both the experiments and the observations. One of the most likely ways to keep SO_2 near the surface during rehydration is by micrometeorite gardening. Gardening of the surface will exhume the dehydrated and SO_2-rich material from below and partially recoat the surface, causing the SO_2 signature to persist for time it takes to overturn, this enriched regolith. We can estimate this time using Cooper et al.'s gardening rate (Cooper et al., 2001), finding that the average time to garden to a depth of

10 cm (estimated depth of the dehydrated regolith) is about 10^5 years or about an order of magnitude longer than the maximum time needed for rehydration. In addition, we note that impacts occur less frequently in the trailing hemisphere compared to the average, so 10^5 years is likely a lower limit. Consequently it is not surprising that the infrared signatures do not show the presence of the monohydrate or a dehydrated surface, even though the SO_2 abundance is high.

5.2. Stability of hydrates on Europa's surface

In Tables 2 and 3, we report destruction cross sections, equilibrium values at high ion fluences, and the half-lives of the three hydrates we studied. For the higher temperature range relevant to Europa (120–130 K), we observe that the ices become more stable as the hydration state of the sulfuric acid is increased, suggesting that these hydrates and higher-order ones, such as the hemihexahydrate ($H_2SO_4{\cdot}6.5H_2O$) and octahydrate ($H_2SO_4{\cdot}8H_2O$), will be stable on geological timescales. In the lower temperature range (86 K), we see that the monohydrate is more stable than the pure sample, as at higher temperatures, but amorphization of the sample makes the interpretation of the loss of the tetrahydrate absorption band problematic, as is mentioned in Section 4.3. However, the overriding trend seen in these experiments is that the mid-IR spectra of all three samples will evolve towards one that resembles the bisulfate ion (HSO_4^-) in the monohydrate, and it is likely that this trend will be followed in the more-highly hydrated acids as well. Whether this change would be manifested in the near-infrared reflectance and whether other processes such as post-irradiation heating (simulating diurnal cycling of the surface) can "undo" some of the spectral changes observed at lower temperatures are two of the questions we hope to address in a future study.

6. Conclusions

We have studied the destruction by 0.8 MeV protons of H_2SO_4, $H_2SO_4{\cdot}H_2O$, and $H_2SO_4{\cdot}4H_2O$ at 10–180 K. During irradiation of our sulfuric acid and monohydrate samples, we detect the formation of water, SO_2, $(S_2O_3)_x$ as well as hydronium and negative ions, mainly HSO_4^- and SO_4^{2-}. Furthermore, we estimate that H_2SO_4 will be destroyed completely given a long enough irradiation, and the ions of the monohydrate will become evident. For the monohydrate, we observed that even though its initial destruction cross section was a factor of 2 larger than that of H_2SO_4, the $H_2SO_4{\cdot}H_2O$ sample actually reached equilibrium at 50% of the starting abundance, indicating that $H_2SO_4{\cdot}H_2O$ is more stable than anhydrous H_2SO_4. Furthermore, the temperature independence for SO_2 production from pure H_2SO_4 compared to the temperature dependence for the hydrate experiments can be explained by OH radicals created in radiolysis of the hydrates, radicals which become mobile at higher temperatures and can more easily destroy SO_2. For $H_2SO_4{\cdot}4H_2O$, we observed that the strong 1065 cm^{-1} absorption of SO_4^{2-} was easily removed by radiolysis at low temperatures, but remained unchanged at higher ones; we speculate that this temperature dependence can be caused by either amorphization or radiolytic destruction, both of which we observed at the lower temperatures. Additionally, we showed that after irradiation at 10 K, the spectra of all three samples appeared similar, and most closely resembled the monohydrate, indicating that the HSO_4^- and H_3O^+ ions may be the most stable ones under irradiation.

Applying our results to the surface of Europa, we speculate that the variations in SO_2 concentrations observed in the chaotic terrains are a result of radiation processing of sulfuric acid in a lower hydration state. Finally, we predict that $H_2SO_4{\cdot}H_2O$ and $H_2SO_4{\cdot}4H_2O$ and other higher hydration states will be stable over geological times in warmer regions of Europa, while in the colder regions the tetrahydrate signature will convert into one that more closely resembles the monohydrate, unless other processes, such as diurnal cycling, induce thermal reactions to allow its reformation.

Acknowledgments

This work was funded by NASA's Planetary Geology and Geophysics program. R.L.H. and M.H.M. also received support through the NASA Astrobiology Institute's Goddard Center for Astrobiology. Steve Brown, Tom Ward, and Eugene Gerashchenko, members of the Radiation Laboratory at NASA Goddard, are thanked for operation and maintenance of the Van de Graaff accelerator.

References

Baklouti, D., Schmitt, B., Brissaud, O., 2008. S_2O, polysulfur oxide and sulfur polymer on Io's surface? Icarus 194, 647–659.
Baragiola, R.A., Atteberry, C.L., Bahr, D.A., Jakas, M.M., 1999. Solid-state ozone synthesis by energetic ions. Nucl. Instrum. Methods Phys. Res. B 157, 233–238.
Boyle, J.W., 1962. The decomposition of aqueous sulfuric acid solution by cobalt gamma rays. Radiat. Res. 17, 427–449.
Carlson, R.W. et al., 1992. Near-infrared mapping spectrometer experiment on Galileo. Space Sci. Rev. 60, 457–502.
Carlson, R.W. et al., 1999a. Hydrogen peroxide on the surface of Europa. Science 283, 2062–2064.
Carlson, R.W., Johnson, R.E., Anderson, M.S., 1999b. Sulfuric acid on Europa and the radiolytic sulfur cycle. Science 286, 97–99.
Carlson, R.W., Anderson, M.S., Johnson, R.E., Schulman, M.B., Yavrouian, A.H., 2002. Sulfuric acid production on Europa: The radiolysis of sulfur in water ice. Icarus 157, 456–463.
Carlson, R.W., Anderson, M.S., Mehlman, R., Johnson, R.E., 2005. Distribution of hydrate on Europa: Further evidence for sulfuric acid hydrate. Icarus 177, 461–471.
Carlson, R.W. et al., 2009. Europa's surface composition. In: Pappalardo, R.T., McKinnon, W.B., Khurana, K. (Eds.), Europa. University of Arizona Press, Tucson, pp. 283–327.
Cassen, P., Reynolds, R.T., Peale, S.J., 1979. Is there liquid water on Europa. Geophys. Res. Lett. 6, 731–734.
Collins, G., Nimmo, F., 2009. Chaotic terrain on Europa. In: Pappalardo, R.T., McKinnon, W.D., Khurana, K. (Eds.), Europa. University of Arizona Press, Tucson, pp. 259–281.
Cooper, J.F., Johnson, R.E., Mauk, B.H., Garrett, H.B., Gehrels, N., 2001. Energetic ion and electron irradiation of the icy Galilean satellites. Icarus 149, 133–159.
Dalton, J.B., 2003. Spectral behavior of hydrated sulfate salts: Implications for Europa mission spectrometer design. Astrobiology 3, 771–784.
Dalton, J.B., 2007. Linear mixture modeling of Europa's non-ice material based on cryogenic laboratory spectroscopy. Geophys. Res. Lett. 34, L21205, doi:10.1029/2007GL023569.
Dalton, J.B., Prieto-Ballesteros, O., Kargel, J.S., Jamieson, C.S., Jolivet, J., Quinn, R., 2005. Spectral comparison of heavily hydrated salts with disrupted terrains on Europa. Icarus 177, 472–490.
Garozzo, M., Fulvio, D., Gomis, O., Palumbo, M.E., Strazzulla, G., 2008. H-implantation in $SO_2$and CO_2 ices. Planet. Space Sci. 56, 1300–1308.
Gillespie, R.J., Robinson, E.A., 1963. Characteristic vibrational frequencies of the SOS group. Spectrochim. Acta 19, 741–746.
Gomis, O., Strazzulla, G., 2005. CO_2 production by ion irradiation of H_2O ice on top of carbonaceous materials and its relevance to the Galilean satellites. Icarus 177, 570–576.
Gomis, O., Strazzulla, G., 2008. Ion irradiation of H_2O ice on top of sulfurous solid residues and its relevance to the Galilean satellites. Icarus 194, 146–152.
Gomis, O., Satorre, M.A., Strazzulla, G., Leto, G., 2004. Hydrogen peroxide formation by ion implantation in water ice and its relevance to the Galilean satellites. Planet. Space Sci. 52, 371–378.
Hapke, B., Graham, F., 1989. Spectral properties of condensed phases of disulfur monoxide, polysulfur oxide, and irradiated sulfur. Icarus 79, 47–55.
Hendrix, A.R., Cassidy, T.A., Johnson, R.E., Paranicas, C., Carlson, R.W., 2011. Europa's disk-resolved ultraviolet spectra: Relationships with plasma flux and surface terrains. Icarus 212, 736–743.
Hibbitts, C.A., McCord, T.B., Hansen, G.B., 2000. Distributions of CO_2 and SO_2 on the surface of Callisto. J. Geophys. Res. 105, 22541–22557.
Hochanadel, C.J., Ghormley, J.A., Sworski, T.J., 1955. The decomposition of sulfuric acid by cobalt gamma rays. J. Am. Chem. Soc. 77, 3215.
Hopkins, A.G., Teng, S., Brown, C.W., 1973. Infrared and raman spectra of the low-temperature products from discharged sulfur dioxide. J. Am. Chem. Soc. 95, 3486–3490.
Horn, A.B., Sulley, K.J., 1999. ATR-IR spectroscopic studies of the formation sulfuric acid and sulfuric acid monohydrate films. Phys. Chem. Chem. Phys. 1, 3801–3806.

Hudson, R.L., Moore, M.H., 1995. Far-IR spectral changes accompanying proton irradiation of solids of astrochemical interest. Radiat. Phys. Chem. 45, 779–789.
Johnson, T.V., McCord, T.B., 1971. Spectral geometric albedo of the Galilean satellites, 0.3 to 2.5 microns. Astrophys. J. 169, 589–594.
Johnson, R.E. et al., 2009. Composition and detection of Europa's sputter-induced atmosphere. In: Pappalardo, R.T., McKinnon, W.D., Khurana, K. (Eds.), Europa. University of Arizona Press, Tucson, pp. 507–527.
Kargel, J.S., Kaye, J.Z., Head, J.W., Marion, G.M., Sassen, R., Crowley, J.K., Ballesteros, O.P., Grant, S.A., Hogenboom, D.L., 2000. Europa's crust and ocean: Origin, composition, and the prospects for life. Icarus 148, 226–265.
Khurana, K.K. et al., 1998. Induced magnetic fields as evidence for subsurface oceans in Europa and Callisto. Nature 395, 777–780.
Kjallman, T., Olovsson, I., 1972. Hydrogen-bond studies. LVIII. The crystal structures of normal and deuterated sulphuric acid tetrahydrate, $(H_5O_2^+)_2SO_4^{2-}$ and $(D_5O_2^+)_2SO_4^{2-}$. Acta Crystallogr. B28, 1692–1696.
Kuiper, G.P., 1957. Infrared observations of planets and satellites. Astron. J. 62, 292–295.
Lane, A.L., Nelson, R.M., Matson, D.L., 1981. Evidence for sulphur implantation in Europa's UV absorption band. Nature 292, 38–39.
Loeffler, M.J., Baragiola, R.A., 2005. The state of hydrogen peroxide on Europa. Geophys. Res. Lett. 32, L17202, doi:10.1029/2005GL023569.
Loeffler, M.J., Hudson, R.L., 2010. Thermally-induced chemistry and the jovian icy satellites: A laboratory study of the formation of sulfur oxyanions. Geophys. Res. Lett. 37, L19201, doi:10.1029/2010GL044553.
Loeffler, M.J., Raut, U., Vidal, R.A., Baragiola, R.A., Carlson, R.W., 2006. Synthesis of hydrogen peroxide in water ice by ion irradiation. Icarus 180, 265–273.
McCord, T.B. et al., 1999. Hydrated salt minerals on Europa's surface from the Galileo near-infrared mapping spectrometer (NIMS) investigation. J. Geophys. Res. 104, 11827–11852.
McCord, T.B., Hansen, G.B., Hibbitts, C.A., 2001a. Hydrated salt minerals on Ganymede's surface: Evidence of an ocean below. Science 292, 1523–1525.
McCord, T.B. et al., 2001b. Thermal and radiation stability of the hydrated salt minerals epsomite, mirabilite, and natron under Europa environmental conditions. J. Geophys. Res. 106, 3311–3319.
Middlebrook, A.M. et al., 1993. Fourier transform-infrared studies of thin H_2SO_4/H_2O films: Formation, water uptake, and solid–liquid phase changes. J. Geophys. Res. 98, 20473–20481.
Moore, M.H., 1984. Studies of proton-irradiated SO_2 at low temperatures implications for Io. Icarus 59, 114–128.
Moore, M.H., Hudson, R.L., 2000. IR detection of H_2O_2 at 80 K in ion-irradiated laboratory ices relevant to Europa. Icarus 145, 282–288.
Moore, M.H., Hudson, R.L., Carlson, R.W., 2007. The radiolysis of SO_2 and H_2S in water ice: Implications for the icy jovian satellites. Icarus 189, 409–423.
Musso, M., Aschauer, R., Asenbaum, A., Vasi, C., Wilhelm, E., 2000. Interferometric determination of the refractive index of liquid sulphur dioxide. Measur. Sci. Technol. 11, 1714–1720.
Nash, D.B., Fanale, F.P., 1977. Io's surface composition based on reflectance spectra of sulfur/salt mixtures and proton-irradiation experiments. Icarus 31, 40–80.
Nash, K.L., Sulley, K.J., Horn, A.B., 2001. Observations on the interpretation and analysis of sulfuric acid hydrate infrared spectra. J. Phys. Chem. A 105, 9422–9426.
Noll, K.S., Johnson, R.E., Lane, A.L., Domingue, D.L., Weaver, H.A., 1996. Detection of ozone on Ganymede. Science 273, 341–343.
Orlando, T.M., McCord, T.B., Grieves, G.A., 2005. The chemical nature of Europa surface material and the relation to a subsurface ocean. Icarus 177, 528–533.
Paranicas, C., Cooper, J.F., Garrett, H.B., Johnson, R.E., Sturner, S.J., 2009. Europa's radiation environment and its effects on the surface. In: Pappalardo, R.T., McKinnon, W.B., Khurana, K. (Eds.), Europa. University of Arizona Press, Tucson, pp. 529–544.
Plonka, A., Szajdzinska-Pietek, E., Kroh, J., 1984. Decay kinetics of hydroxyl radicals in frozen aqueous systems. Rad. Phys. Chem. 23, 583–587.
Sack, N.J., Johnson, R.E., Boring, J.W., Baragiola, R.A., 1992. The effect of magnetospheric ion bombardment on the reflectance of Europa's surface. Icarus 100, 534–540.
Salama, F., Allamandola, L.J., Witteborn, F.C., Cruikshank, D.P., Sandford, S.A., Bregman, J.D., 1990. The 2.5–5.0 micron spectra of Io – Evidence for H_2S and H_2O frozen in SO_2. Icarus 83, 66–82.
Schenk, P., 2010. Atlas of the Galilean Satellites. Cambridge Univ. Press, Cambridge.
Schenk, P.W., Steudel, R., 1965. New findings in the chemistry of the lower oxides of sulfur [1]. Angew. Chem. Int. Edit. 4, 402–409.
Schriver-Mazzuoli, L., 2003. Infrared spectra of SO_2 and SO_2:H_2O ices at low temperature. J. Mol. Struct. 644, 151–164.
Schriver-Mazzuoli, L., Schriver, A., Chaabouni, H., 2003. Photo-oxidation of SO_2 and of SO_2 trapped in amorphous water ice studied by IR spectroscopy. Implications for Jupiter's satellite Europa. Can. J. Phys. 81, 301–309.
Siegel, S., Baum, L.H., Skolnik, S., Flournoy, J.M., 1960. Observations of the thermal behavior of radicals in gamma-irradiated ice. J. Chem. Phys. 32, 1249–1256.
Spencer, J.R., Calvin, W.M., 2002. Condensed O_2 on Europa and Callisto. Astron. J. 124, 3400–3403.
Spencer, J.R., Klesman, A., 2001. New observations of molecular oxygen on Europa and Ganymede. Bull. Am. Astron. Soc. 33, 1125 (abstract).
Spencer, J.R., Tamppari, L.K., Martin, T.Z., Travis, L.D., 1999. Temperatures on Europa from Galileo photopolarimeter–radiometer: Nighttime thermal anomalies. Science 284, 1514–1516.
Spinks, J.W.T., Woods, R.J., 1990. An Introduction to Radiation Chemistry. Wiley and Sons, New York.
Steudel, R., Steudel, Y., 2004. The thermal decomposition of S_2O forming SO_2, S_3, S_4, and S_5O – An ab initio MO study. Eur. J. Inorg. Chem. 2004, 3513–3521.
Strazzulla, G., Johnson, R.E., 1991. Irradiation effects on comets and cometary debris. In: Newburn, R.L., Neugebauer, M., Rahe, J.H. (Eds.), Comets in the Post Halley Era. Dordrecht, Kluwer, pp. 243–275.
Strazzulla, G., Baratta, G.A., Leto, G., Foti, G., 1992. Ion-beam-induced amorphization of crystalline water ice. Europhys. Lett. 18, 517–522.
Strazzulla, G., Baratta, G.A., Leto, G., Gomis, O., 2007. Hydrate sulfuric acid after sulfur implantation in water ice. Icarus 192, 623–628.
Taesler, I., Olovsson, I., 1968. Hydrogen bond studies. XXI. The crystal structure of sulphuric acid monohydrate. Acta Crystallogr. B24, 299–304.
Teolis, B.D., Loeffler, M.J., Raut, U., Famá, M., Baragiola, R.A., 2006. Ozone synthesis on the icy satellites. Astrophys. J. 644, L141–L144.
Teolis, B.D., Loeffler, M.J., Raut, U., Famá, M., Baragiola, R.A., 2007. Infrared reflectance spectroscopy on thin films: Interference effects. Icarus 190, 274–279.
Warren, S.G., Brandt, R.E., 2008. Optical constants of ice from the ultraviolet to the microwave. J. Geophys. Res. 113, D14220.
Zhang, R., Wooldridge, P.J., Abbatt, J.P.D., Molina, M.J., 1993. Physical chemistry of the H_2SO_4/H_2O binary system at low temperatures: Stratospheric implications. J. Phys. Chem. 97, 7351–7358.
Ziegler, J.F., 2010. Stopping and Range of Ions in Matter SRIM2010. <www.srim.org>.